Hindawi
Journal of Nanomaterials
Volume 2021, Article ID 5570866, 14 pages
https://doi.org/10.1155/2021/5570866

Research Article

Effect of NH_3 Alkalization and MgO Promotion on the Performance of Ni/SBA-15 Catalyst in Combined Steam and Carbon Dioxide Reforming of Methane

Phan H. Phuong,[1,2] Luu C. Loc,[1,2,3,4] Nguyen Tri,[3,4] Nguyen P. Anh,[3] and Ha C. Anh[1,2,4]

[1]*Vietnam National University Ho Chi Minh City, Linh Trung Ward, Thu Duc District, Ho Chi Minh City, Vietnam*
[2]*Ho Chi Minh City University of Technology (HCMUT), 268 Ly Thuong Kiet Street, Ho Chi Minh City, Vietnam*
[3]*Institute of Chemical Technology, Vietnam Academy of Science and Technology, Ho Chi Minh City, Vietnam*
[4]*Graduate University of Science and Technology, Vietnam Academy of Science and Technology, Hanoi, Vietnam*

Correspondence should be addressed to Luu C. Loc; lcloc@ict.vast.vn

Received 8 January 2021; Revised 30 March 2021; Accepted 17 April 2021; Published 17 May 2021

Academic Editor: Nguyen Duc Cuong

In this work, 31.4 wt.% Ni/SBA-15 (Ni/SBA-15) nonpromoted and alkalized with ammonia solution and by MgO promoter catalysts were prepared and used for combined steam and CO_2 reforming of CH_4 (bireforming). Effect of concentration of ammonia solution ($NH_{3(aq)}$) (10–25 vol.%) and Mg content (3–12 wt.%) on the properties of the Ni/SBA-15 catalysts was investigated by low-angle and powder X-ray diffraction (XRD), N_2-BET isothermal adsorption, SEM, TEM, EDS mapping, H_2-TPR, and CO_2-TPD methods. The performance of the catalysts in bireforming was assessed in the temperature range of 550–800°C. The enhancement of dispersion of NiO particles, reducibility, and basicity of alkalized Ni/SBA-15 catalysts were responsible for improving the catalytic performance of this catalyst. The results revealed that the Ni/SBA-15 treated with 15-25% $NH_{3(aq)}$ solution and promoted with 3-9% Mg exhibited high activity for CH_4 conversion. Meanwhile, Ni6Mg/SBA-15 showed the highest CO_2 conversion. Among tested catalysts, Ni/SBA-15-20NH_3 and Ni9Mg/SBA-15 samples had an almost equal activity with a CH_4 conversion of nearly 97% and a CO_2 conversion of about 84% at 700°C thanks to its moderate affinity with both CO_2 and CH_4. However, the H_2/CO ratio of the product mixture remained at 2.02 on the Ni/SBA-15-20NH_3 catalyst and almost 1 on the Ni9Mg/SBA-15 sample. These results might be related to the fact that the alkalization of the Ni/SBA-15 catalyst by $NH_{3(aq)}$ solution had an advantage over using MgO because side reactions were unlikely to occur.

1. Introduction

The rapid increase in emissions of major greenhouse gases such as CO_2 and CH_4 in the last decade has seriously affected climate change and the living environment in the world. Besides, syngas, the variable mixture of carbon monoxide and hydrogen, is an important intermediate for downstream processes in the chemical industry. Including many benefits for producing syngas from available natural gas reservoirs, along with the consumption of two main greenhouse gases, bireforming of CH_4 using CO_2 and H_2O (reaction (1)) is the most suitable method with extensive application in the chemical industry [1]:

$$3CH_4 + CO_2 + 2H_2O \longrightarrow 4CO + 8H_2, \quad \Delta H_{298} = +220\ \text{kJ/mol} \tag{1}$$

The bireforming process (BRM) (reaction (1)) consists of two reactions: dry reforming (DRM) (reaction (2)) and steam reforming (SRM) (reaction (3)):

$$CH_4 + CO_2 \rightleftharpoons 2CO + 2H_2, \quad \Delta H_{298} = +247.3\ \text{kJ/mol} \quad (2)$$

$$CH_4 + H_2O \rightleftharpoons CO + 3H_2, \quad \Delta H_{298} = +206.3\ \text{kJ/mol} \quad (3)$$

As can be seen from reactions (1) and (2), the enthalpy at 298 K of DRM is +247.3 kJ/mol, 1.122 times higher than BRM. This means that, as an endothermic reaction, the combined CO_2 and steam reforming of methane (Equation (1)) consumes less energy than DRM (Equation (2)). Furthermore, this combination shows the most desirable stoichiometry of H_2 and CO, completely suitable for the Fischer-Tropsch synthesis process. By feeding CO_2 and steam simultaneously, the products' ratio can be controlled by adjusting the $CH_4/CO_2/H_2O$ ratio of the feedstock [2]. Moreover, one of the disadvantages of steam reforming methane is the generation of large amounts of CO_2 in the side reaction

$$CO + H_2O \rightleftharpoons CO_2 + H_2, \quad \Delta H^o_{298K} = -41\ \text{kJ/mol} \quad (4)$$

In a bireforming reaction, this problem was overcome. In addition, adding H_2O to the dry reforming reaction (2), to create a bireforming reaction (1), has limited coke deposition—the biggest disadvantage of CO_2 reforming of methane, thanks to reaction (5) [3]:

$$C + H_2O \rightleftharpoons CO + H_2, \quad \Delta H^o_{298K} = +131.3\ \text{kJ/mol} \quad (5)$$

For these reasons, presently, bireforming is receiving great attention for converting natural gas into synthetic gas.

Metals in the VIII B group, especially Ni, Ru, Rh, Pd, Ir, and Pt, have been reported to be highly active in CH_4 reforming processes. Despite higher activity and stability, the usage of noble metals is not preferred due to their high cost and less availability. Among other transition metals, Ni possesses high reactivity towards conversion of hydrocarbons [4], photocatalytic water splitting [5], and the hydrogen and the oxygen evolution reaction [6]. In general, supported Ni catalysts are commercially used in steam reforming of CH_4 because of the cheap price and good performance compared to the ones with noble metals [7, 8]. However, coke formation and metal sintering have been making this process inapplicable commercially until recently. Hence, metal dispersing and coke resistance improvement of Ni-based catalyst has been attracting attention.

In our previous study [9], nanosized NiO/SBA-15 catalysts with NiO crystallite size in the range of 12.9 to 18.3 nm were successfully prepared. In this catalytic system, there are 5–6 nm NiO particles dispersed inside the pores and the NiO particles of 20–50 nm distributed on the surface of SBA-15 when Ni content was 23.5–39.2 wt.%. Dispersion of metallic sites into the pores could prevent Ni from sintering and metal loss during reaction. The high dispersion of NiO in the Ni/SBA-15 catalyst is caused by the unique properties of SBA-15 such as uniform pores with large diameters (5.3–6.0 nm), high porosity, and high specific surface area (613 m^2/g). The reduced catalysts have high activity in bireforming reaction, reaching 86% CH_4 and 77% CO_2 converted at 700°C or 90.5% and 80%, respectively, at 800°C. The catalysts work stably for hundreds of hours due to the presence of weak and strong Lewis basic sites which limit coke formation and increase CO_2 adsorption. Similarly, Zhang et al. [10] reported that 12.5% NiO/SBA-15 catalyst had CH_4 and CO_2 conversion at 800°C of 89% and 85%, respectively, and could remain its activity over 600 hours time-on-stream (TOS) in CO_2 methane reforming. As a result, SBA-15 is believed to be potential support for nickel catalyst in the methane bireforming process.

Deactivation of Ni/SBA-15 catalyst in dry reforming of CH_4 has been addressed to coke deposition rather than sintering of Ni particles [10]. One of the most important factors affecting coke deposition during the reaction is the basicity of catalysts [11]. Coke formation could be reduced or even inhibited when the active metal is dispersed on the metal oxide support with Lewis basic sites. Many studies show that the addition of alkali and alkaline earth metals could change the nature of supports, leading to a reduction of coke formation and an increase of CO_2 adsorption [12]. For example, adding a basic Lewis promoter such as alkali metal oxides (Na_2O, K_2O), alkaline earth (CaO, MgO), or weak base (NH_4OH) reduces coke deposition and metal sintering of Ni/Al_2O_3, Ni/SiO_2, and NiO/SBA-15 catalysts [12–14].

Danilova et al. [15] suggested that the structural similarity of NiO and MgO led to the formation of a solid solution in the form of a thin layer, surrounding the Ni particles that increased catalyst stability and reduced carbon deposition. Wang et al. [16] demonstrated that in the MgO-modified Ni/SBA-15 catalyst synthesized by the coimpregnation method, the MgO particles covered the walls of channels of SBA-15. Besides, the catalyst basicity increased and the Ni dispersion was improved, leading to an enhancement in chemical adsorption of CO_2. As a result, the activity and the coke resistance of the catalyst in the dry reforming reaction were improved. In addition, Alipour et al. [17] reported that adding MgO to the nickel catalyst promoted the catalyst reducibility that enhanced CH_4 conversion and coke resistance. NiO-MgO bonding was useful in preventing Ni particle sintering; carbon deposits and these facts have been accepted in many studies [15, 18, 19].

Recently, another promoter considered to be examined was NH_4OH. Previous researches used NH_4OH as a pH controller for some processes [20, 21], but NH_4OH could also be used as a promoter thanks to its basicity to enhancing some characteristics of the catalyst. This property was believed to reduce the acidic sites which would improve catalyst activity, limit coke formation, and stabilize catalyst. Modification of SBA-15 by attaching the $-NH_2$ group to its structure improved the structural stability and increased content of amino as well as basic sites [22]. Hao et al. [23] indicated that alkalization increased catalytic activity and coke resistance of the supported Co/Al_2O_3 catalyst.

However, to the best of our knowledge, the impact of treatment with aqueous NH_3 step in catalyst preparation or promoting catalysts by MgO on the activity of Ni/SBA-15 catalyst in bireforming has not been carried out so far. In our previous investigation [9], it was reported that NiO/SBA-15 catalyst contained 31.4 mass% Ni (Ni/SBA-15), exhibiting higher activity than other Ni/SBA-15 samples. The conversion of CH_4 and CO_2 on this catalyst in

bireforming (BRM) reached 90% and 76%, respectively, at 700°C. In this study, the effect of NH_3 alkalization or promotion by MgO on catalytic activity of Ni/SBA-15 catalyst in BRM reaction was investigated and optimized.

2. Materials and Methods

SBA-15 was prepared by the method described in the work [9]. To prepare SBA-15 alkalized with ammonia solution (SBA-15-NH_3), 2 grams of SBA-15 was put into beakers containing 50 ml $NH_{3(aq)}$ solution with various concentrations, 10%, 15%, 20%, and 25% in volume, respectively. These mixtures were then placed in an autoclave at 160°C for 10 h. After that, they were washed with distilled water and dried at 120°C for 2 h.

Then, NiO supported on SBA-15-NH_3 catalysts were prepared by impregnating $Ni(NO_3)_2$ solution on SBA-15-NH_3 according to the procedure described in reported work [9]. The Ni content in the catalysts was fixed at 31.4 wt.% (or 40 wt.%NiO). The obtained samples were calcined in air at 800°C for 0.5 h and symbolized as follows, Ni/SBA-15-*a* NH_3, where *a* represents concentration of ammonia solution used in preparation of alkalized SBA-15 support. Meanwhile, NiO supporting SBA-15 promoted by MgO catalysts were formed by using coimpregnation of $Ni(NO_3)_{2(aq)}$ and $Mg(NO_3)_{2(aq)}$ solution on support SBA-15. The amount of $Mg(NO_3)_{2(aq)}$ solution used is varied to obtain samples with different Mg contents (3–12 wt.%). After that, the samples were calcined at 800°C for 0.5 h and were denoted as Ni*b* Mg/SBA-15, where *b* performs Mg content. All the samples were then reduced *in situ* in 40 mol% H_2/N_2 gas mixture (3 L/h) at 800°C for 2 h before reaction.

The physicochemical properties of the catalysts were studied by several methods such as XRD (Bruker D2 Phaser powder diffractometer), N_2-BET isothermal adsorption (Nova Station B, Quantachrome NovaWin Instrument), scan electron microscopy (FE–SEM JEOL 7401 instrument), transmission electron microscopy (TEM on the TEM JEM 1400 of JEOL USA instrument), EDS mapping on JEOL JST-IT 200 instrument, hydrogen temperature-programmed reduction (H_2-TPR), and the carbon dioxide temperature-programmed desorption (CO_2-TPD). Both H_2-TPR and CO_2-TPD were carried out on a microreactor with a sample of 50 mg using a Gas Chromatograph GOW-MAC 69-350 with a thermal conductivity detector (TCD). The activity of catalysts for bireforming was tested in a microflow reactor under atmospheric pressure at a temperature of 550–800°C as described in detail in our previous paper [9]. Briefly, a catalyst sample of 0.2 grams, the feed flow rate of 6 L/h, CH_4 concentration in feed of 3 mol.%, and the molar ratio of $CH_4 : CO_2 : H_2O$ in feed of 3 : 1.2 : 2.4 was used in the investigation.

3. Results and Discussion

3.1. Physicochemical Characteristics of Catalysts. The properties of bare SBA-15 support are showed detailed in our previous paper [9]. Briefly, three intensive main diffraction peaks at 2θ of 0.90°, 1.60°, and 1.84°, indexed as the (100), (110), and (200) reflections, respectively, appearing in the low-angle XRD pattern (Figure 1(a)), prove that two-dimensional, ordered hexagonal mesostructure SBA-15 was successfully prepared [24]. The SEM image (Figure 1(b)) showed that SBA-15 was prepared in a porous cocoon diameter of hundred nm. N_2 adsorption-desorption profiles of the synthesized SBA-15 are presented in Figure 1(c). According to the IUPAC classification, the profile of the sample belonged to the IV type isotherm curve with the H1 hysteresis loop in a P/P_0 range of 0.45–0.7, which was a characteristic of mesoporous materials. Hysteresis was observed for reasonably large pores ($d \geq 4$ nm), and these pores showed capillary condensation and evaporation at values for $P/P_0 > 0.45$ [25]. The H1 type hysteresis of obtained SBA-15 indicated the well-organized materials, associating with the presence of cylindrical pores. Moreover, the small inclination of hysteresis indicated that the obtained pores were uniform. This result was further confirmed by the TEM image of synthesized SBA-15 reported in our previous paper [26]. The diameter of the channels of SBA-15, determined from the N_2 adsorption isotherms (Figure 1(d)) and TEM analysis [26], was approximately 6.08 nm. The specific surface area and pore volume of the synthesized SBA-15, determined from the N_2 adsorption isotherm, were 639.1 $m^2 \cdot g^{-1}$ and 0.65 $cm^3 \cdot g^{-1}$, respectively. Therefore, NiO were easily dispersed into the channel system of SBA-15, as indicated in Figure 2(a').

The reducibility of supports was characterized by the H_2-TPR method. It was found from Figure 1(e) that there were no reduction peaks for SBA-15 and NH_3-treated SBA-15 supports in the temperature range from 100 up to 900°C. The basicity of supports and catalysts was evaluated via CO_2-TPD characterization. It was reported that there were three CO_2-TPD peaks observed in the temperature ranges of 100–200, 300–400, and 600–800°C, attributed to weak, moderate, and strong basic sites, respectively [27]. The two CO_2-TPD peaks of SBA-15 and SBA-15-NH_3 at 100–200°C and 500–700°C were attributed to weak and strong basic sites, respectively. The same result was reported by Zhang et al. [27]. The presence of weak basic sites (100–200°C) and strong basic sites (600–700°C) on SBA-15 was explained as follows. At the heating temperature of 550°C for 2 hours, there still existed H_2O and Cl^- ions in the structure of SBA-15, which were Lewis bases. The CO_2-TPD pattern of the ammonia-treated support, SBA-15-NH_3, was similar, including the characteristic peaks for weak and strong basic sites. Heating ammonia in glass tubes at various temperatures, Perman and Atkinson found that decomposition began under the most favourable circumstances at 500°C [28]. Then, on the alkalized support, there existed NH_3, which almost did not dissociate to N_2 and H_2 at drying temperature 120°C for 2 hours, providing additional Lewis basic sites.

The wide-angle XRD patterns of the obtained catalysts are indicated in Figure 3. The spreading peak located at about 20-25° was accredited to the silica frameworks belonging to SBA-15 support for all catalysts [29]. The XRD patterns of NH_3-modified SBA-15 supported NiO (Figure 3(a)), and MgO-promoted NiO/SBA-15 catalysts (Figure 3(b)) showed that all catalysts exhibited diffraction peaks with high

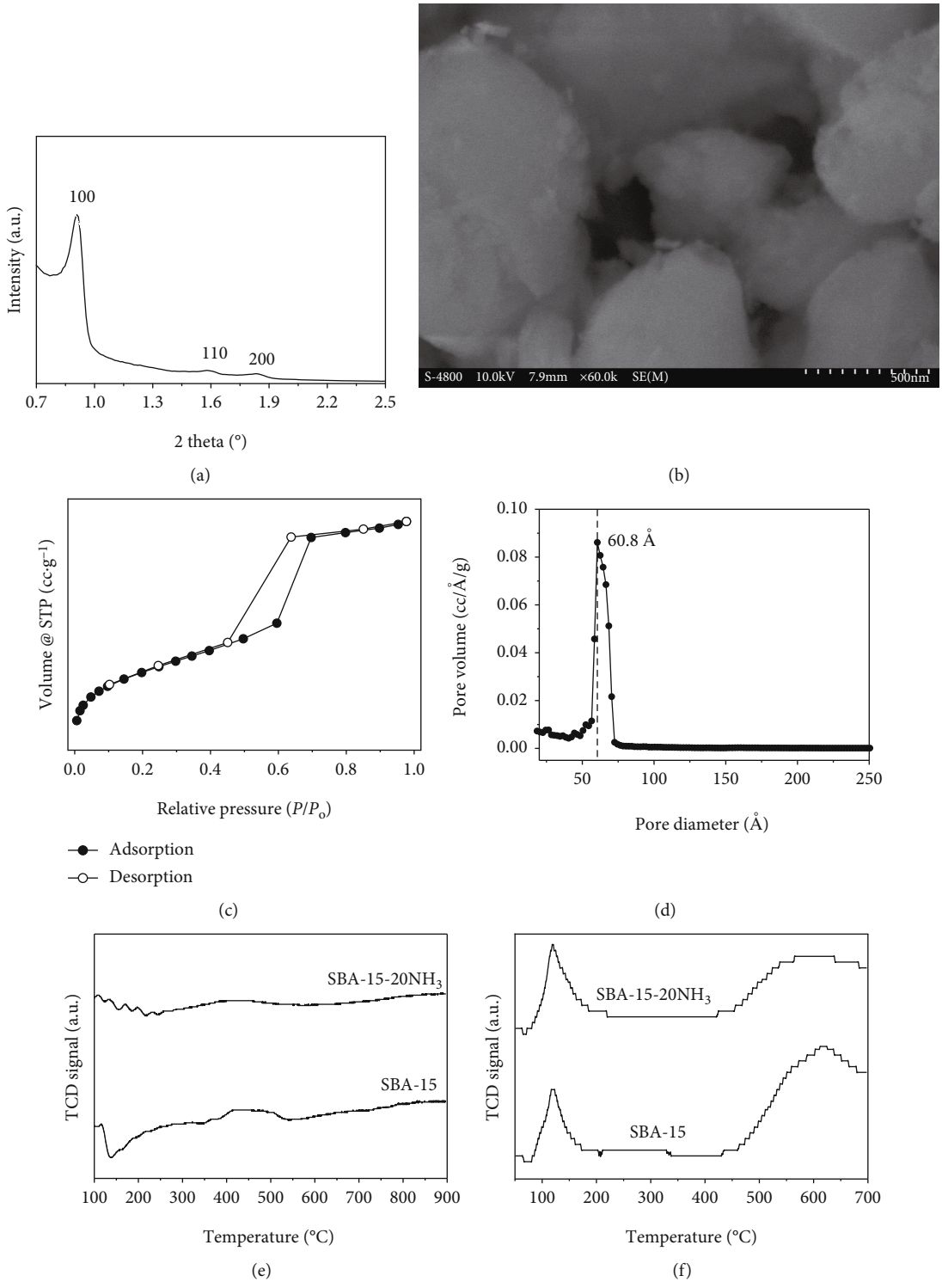

FIGURE 1: The narrow-angle XRD pattern (a) [9] and physicochemical properties of synthesized SBA-15 support: SEM image (b), N_2 isotherm (c), pore distribution (d), H_2-TPR profiles (e), and CO_2-TPD pattern (f).

intensity at $2\theta = 37.3^\circ$, 43.2°, 62.9°, 76°, and 79.3° corresponding to (101), (200), (220), (311), and (222) plans of a face-center cubic crystalline NiO structure in all catalysts [30]. Moreover, all of the peaks were highly apparent at high intensity. This meant that NiO appeared as a high-crystalline state. Besides, the peaks for the NiO phase in alkalized catalysts were more intense than that of the bare catalyst, Ni/SBA-15. It was proposed that NiO particles were not dispersed homogeneously over the mesopores of SBA-15 for alkalized samples [31]. Based on XRD patterns, the average crystallite

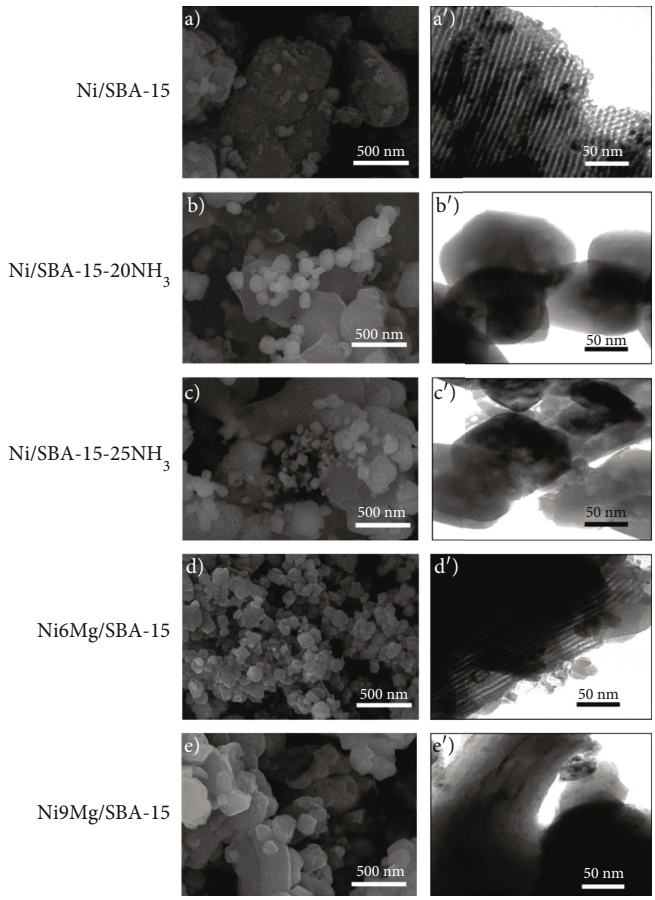

Figure 2: SEM images (a–e) and TEM images (a'–e') of the catalysts.

size of NiO (d_{cry}) could be calculated through the Scherrer equation [32] at $2\theta = 43.2°$, which is shown in Table 1. As seen, the size of NiO crystals increased from 18.4 nm in non-promoted catalyst to 18.5-21 nm in the MgO-promoted ones and to 30–40 nm in ammonia-alkalized samples (Table 1). In particular, no characteristic peaks of MgO crystallites were detected in all samples containing 3–12% Mg. This fact suggested a high dispersion of Mg oxides on mesoporous silica or a formation of Ni-Mg-O solid solution [33].

On the SEM image of the nonmodified sample Ni/SBA-15 catalyst (Figure 2(a)), the SBA-15 cocoon diameter of 200-400 nm and spherical particle size of ten nm sticking on the cocoon surface were found. The highly ordered hexagonal structure of the SBA-15 was clearly observed on the TEM image of this catalyst (Figure 2(a')). In addition, the nanosized NiO particles in the channels of SBA-15 and some large clusters on the outer surfaces were shown in the TEM image of the Ni/SBA-15 sample (Figure 2(a')). This meant that the size of inside NiO particles was around 6 nm and of outside NiO bulk was almost ten nm.

The cocoon shape of SBA-15 was still observed on SEM images of all alkalized samples (Figures 2(b)–2(e)). It could be seen from Figures 2(b) and 2(c) that, for NH_3-alkalized Ni/SBA-15 samples, cocoons had smaller size and are less porous than nonmodified Ni/SBA-15 and some particles had been broken down. The SEM image of the MgO-promoted samples (Figures 2(d) and 2(e)) was characterized by many bright spherical particles with size of 10-50 nm appearing on the surface of SBA-15 cocoons. In addition, the ordered mesostructure was still observed on the TEM images (Figures 2(d') and 2(e')) of these samples. On the TEM image of the MgO-promoted samples, besides the dark particles being similar to those of the Ni/SBA-15 sample (Figure 2(a')), the light-colored particles were also observed. Both types of particles appeared both in the structural channel and on the outer surface of SBA-15 support. This proved the existence of particles with different compositions on the NiMg/SBA-15 catalyst. Specifically, dark-colored particles could be assigned to NiO while light-colored particles were responsible for the MgO or the NiO-MgO mixture. Meanwhile, as depicted in Figures 2(b') and 2(c'), the ordered mesoporous structure was not observed on TEM images of NH_3-alkalized Ni/SBA-15 samples. This was possibly due to the damage of thin pore walls of SBA-15 support in ammonia solution. On the TEM image of the NH_3-modified samples (Figures 2(b') and 2(c')), the light-colored particles, assigned to NiO particles distributed in the porous structure of the material and the dark color thin layer, which might be derived from NH_3, could be seen.

EDS mapping of catalysts (Figure 4) indicated an evenly and highly dispersed form of all species on all catalysts. The elemental composition indicated in the EDS mapping to

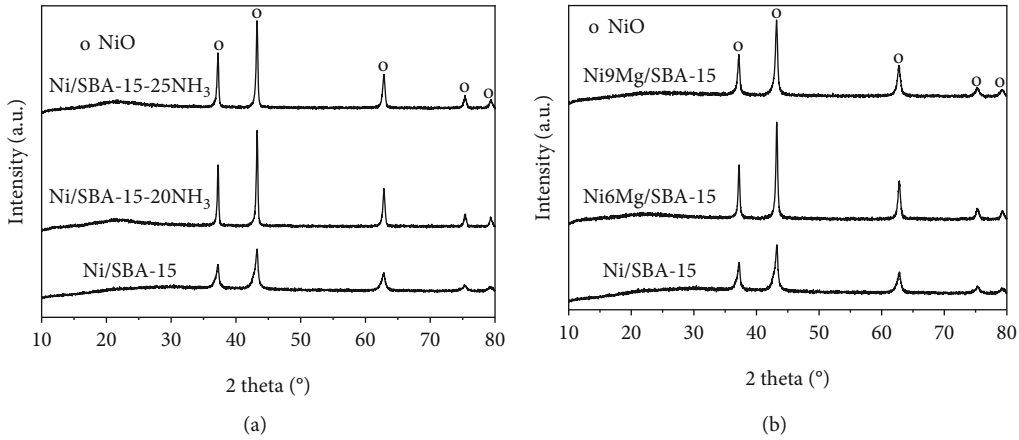

Figure 3: XRD patterns of NiO/SBA-15 catalysts alkalized with $NH_{3(aq)}$ (a) and NiO/SBA-15 catalysts promoted by MgO (b).

Table 1: The structural properties of the catalysts.

Catalysts	S_{BET} [a] (m^2/g)	d_{pore} [a] (nm)	V_{pore} [a] (cm^3/g)	d_{cry} [b] (nm)	T_{max} [c] (°C)	m_{Ni^o} [c] (a.u.)	m_{CO_2} [d] (a.u.)
Ni/SBA-15	232.6	6.08	0.29	18.35	369, 450, and 620	1	1
Ni/SBA-15-15NH_3	—	—	—	—	340	1.8	1.2
Ni/SBA-15-20NH_3	24.89	2.50	0.02	40.8	331	1.8	1
Ni/SBA-15-25NH_3	27.42	2.54	0.02	30.0	330	1.9	1.2
Ni3Mg/SBA-15	—	—	—	—	392, 788	0.89	1
Ni6Mg/SBA-15	36.5	2.14	0.02	21.0	385, 760	0.73	2
Ni9Mg/SBA-15	27.5	1.64	0.01	18.5	360, 440, and 586	1.07	4

[a]BET surface (S_{BET}), average pore diameter (d_{pore}), and total pore volume (V_{pore}) were obtained from N_2 adsorption isotherm analysis. [b]NiO crystal size (d_{cry}) was obtained from XRD patterns at $2\theta = 43.2°$. [c]The maximal reduction temperature (T_{max}) and the number of reduced Ni^o (m_{Ni^o}), based on H_2 consumption, were obtained from H_2-TPR results. [d]The desorbed CO_2 amount (m_{CO_2}) was obtained from the results of CO_2-TPD results of activated samples.

some extent was matched with the loading value, proving that the method of catalysts' preparation was suitable. On the Ni/SBA-15 catalyst, the elemental content of Si (28.4%) was approximate to the loading value (28.0%) while the oxygen content was slightly higher (46.8% vs. 40%) and of Ni was slightly lower (24.8 vs. 31.4%). This might be related to the formation of some large clusters on the outer surfaces of the catalyst, as seen in the TEM image, reducing the Ni content. Meanwhile, the Ni content of the two alkalinized catalysts was higher than the calculated value, demonstrating the positive effect of the alkalization on Ni dispersion. The highest Ni content was achieved on the MgO-modified catalyst (Ni6Mg/SBA-15), reaching 40.6% (compared to 31.4% calculated value). This fact showed that Mg was a highly effective additive for improving Ni dispersion. In this sample, the Mg content was approximate to the expected value (5.3% vs. 6.0%) although MgO was not detected on the XRD pattern (Figure 3(b)). This fact proved that highly dispersed MgO was successfully introduced into SBA-15. Meanwhile, the content of Si and O in this sample was lower than the calculated values, respectively, 20.1 vs. 26.7% and 34.0% vs. 39.3%. This might be related to the highest density of active metal particles on the SBA-15 surface as found on the TEM image of sample Ni6Mg/SBA-15 (Figure 2(d)). On the $NH_{3(aq)}$-treated catalyst (Ni/SBA-15-20NH_3), the elemental composition of the EDS mapping was the most matched with the calculated values. Specifically, the components of Si, O, and Ni are 25.1% vs. 28%, 39.9% vs. 40.6%, and 32.3% vs. 31.4%, respectively. In particular, the content of N in this sample was determined to be 2.7%, proving that N was included in the Ni/SBA-15 catalyst. This was explained as follows. Although NH_3 was almost completely dissociated to N_2 and H_2 at 650°C on supported nickel catalysts [34], a small residual of ammonia was found even at 700°C and 800°C in calcination [35].

The alkalization of Ni/SBA-15 with NH_3 and with MgO promoter led to a sharp decrease in pore diameter, pore volume, and specific surface area. In particular, the specific surface area value dropped from 232.6 m^2/g of Ni/SBA-15 to 25–37 m^2/g, the pore diameter decreased from 6 nm to 2 nm, and the pore volume fell from 0.29 to 0.01–0.02 cm^3/g (Table 1). A sharp decrease in pore diameter and pore volume might be related to coverage of the channel walls of SBA-15 by MgO particles [16] and attachment of NH_3 residual to the structural channel of support as seen on TEM images. Consequently, the specific surface area of the catalysts was drastically reduced. However, the pore diameter of the alkalized catalysts was still being favourable for the diffusion of CH_4 and CO_2 into the pores, as their kinetic diameter was 0.38 and 0.44 nm, respectively. Besides, as seen from SEM images,

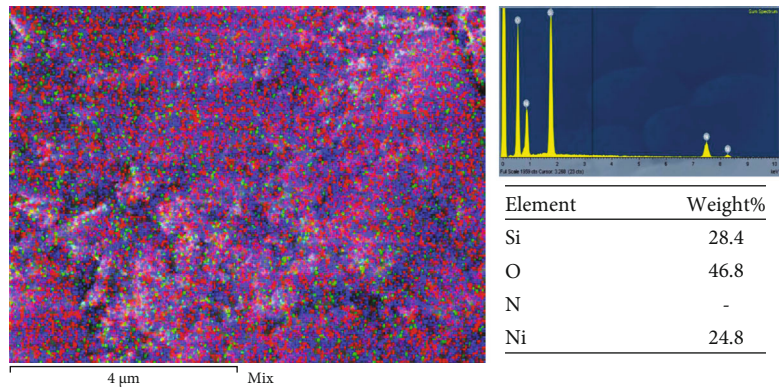

Element	Weight%
Si	28.4
O	46.8
N	-
Ni	24.8

Si–White; O–Green; Ni–Red

(a)

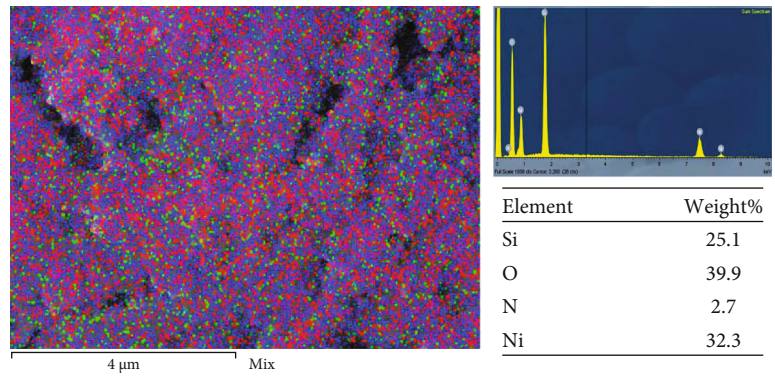

Element	Weight%
Si	25.1
O	39.9
N	2.7
Ni	32.3

Si–White; O–Green; N–Blue; Ni–Red

(b)

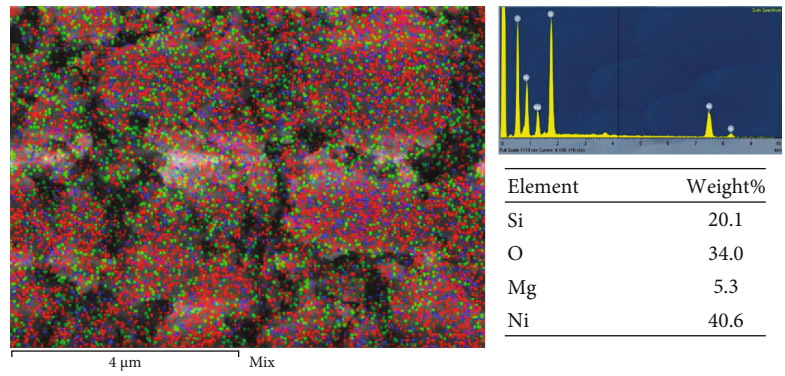

Element	Weight%
Si	20.1
O	34.0
Mg	5.3
Ni	40.6

Si–White; O–Green; Mg–Blue; Ni–Red

(c)

Figure 4: EDS mapping of catalysts: Ni/SBA-15 (a), Ni/SBA-15-20NH_3 (b), and Ni6Mg/SBA-15 (c).

Ni6Mg/SBA-15 showed the smallest size. Consequently, this sample had the highest specific surface area among the alkalized catalysts.

H_2-TPR profiles of the Ni/SBA-15 catalysts modified by $NH_{3(aq)}$ or MgO are depicted in Figure 5. The H_2-TPR pattern of the Ni/SBA-15 catalyst showed three reduction peaks. The former strongest peak is at $T_{max,1} = 372°C$, assigned to the reduction of free, bulky NiO [36, 37]. The second very weak reduction peak is at $T_{max,2} = 450°C$, representing the reduction of the weak interacted NiO-support species, and the third one is at $T_{max,3} = 620°C$, being attributed to the reduction of some forms of Ni^{2+} ions strongly interacting with support [27] and/or reduction of small clusters of Ni^{2+} in pores [38]. Compared to the Ni/SBA-15 catalyst, the NH_3-modified samples presented the shifting of the first reduction peak towards lower temperature, $T_{max,1}$ = 330-355°C, while the other two reduction peaks almost disappeared. This was consistent with the fact that only one type of active phase particle was observed on the TEM image (Figures 2(b') and 2(c')). Besides, the higher the

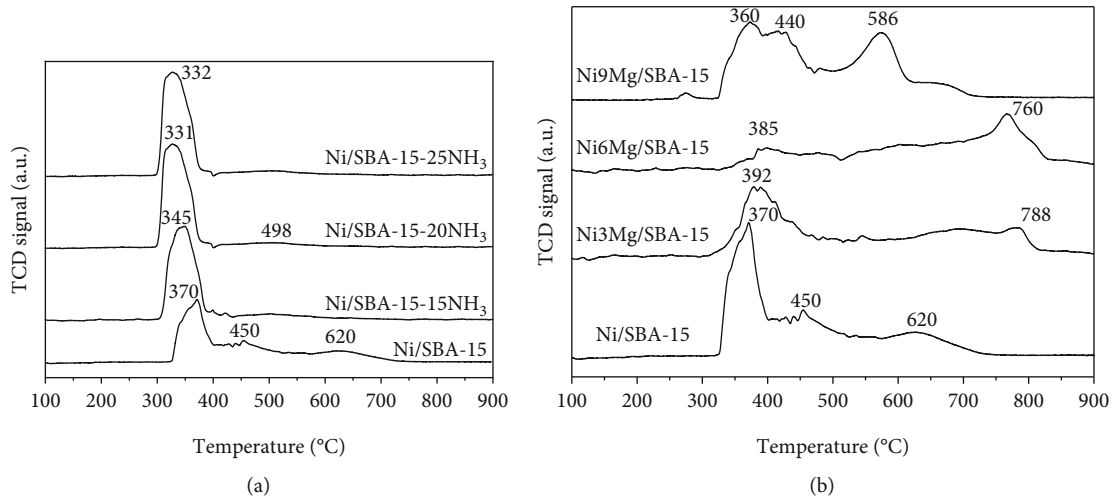

FIGURE 5: H_2-TPR profiles of NiO/SBA-15 catalysts alkalized with $NH_{3(aq)}$ (a) and NiO/SBA-15 catalysts promoted by MgO (b).

concentration of NH_3 solution, the more shift of reduction peaks towards the lower temperature was observed. Moreover, the area of the lower temperature reduction peak increased about doubles when nonmodified and modified catalysts were compared. That means the alkalization of SBA-15 with $NH_{3(aq)}$ solution led to an enhancement of reducibility of the Ni/SBA-15 catalyst, whereby the catalytic activity should be improved.

The characteristics of the H_2-TPR pattern of NiMg/SBA-15 catalysts (Figure 5(b)) were dependent on the MgO loading content. When the low-Mg content (3–6%) was added, the H_2-TPR profiles of NiMg/SBA-15 catalysts showed two reduction peaks. The shifting of the first reduction peak towards higher temperature ($T_{max,1}$ = 392 and 385°C) compared to the Ni/SBA-15 sample demonstrated an enhancement on the metal-support interactions [39]. The second peak in the H_2-TPR profile, at 760–788°C, was attributed to the reduction of some forms of Ni^{2+} ions deeply located in the MgO lattice which exhibited a strong interaction [27]. The area ratio of the second reduction peak to the first reduction peak rose with the increase of MgO loading content. This indicated that the more MgO added to the catalyst, the more the number of interacted NiO-MgO species formed. Meanwhile, the H_2-TPR pattern of the Ni9Mg/SBA-15 sample consists of three reduction peaks centered at 360, 440, and 586°C. There was no reduction peak above 700°C while a reduction peak at around 600°C appeared on the TPR profile of the Ni9Mg/SBA-15 catalyst. This new reduction peak could be assigned to the strong interaction of NiO with bare MgO [13], which formed when the loading MgO was in excess. The catalysts alkalized with NH_3 solution showed a higher number of reduced Ni^o as compared to the catalysts modified by the MgO additive. This might be related to the fact that the catalysts alkalized with NH_3 solution had a homogeneous dispersion of the elements throughout the catalyst since the elemental composition from EDS data was well matched with the calculated value.

The profiles of CO_2-TPD of modified Ni/SBA-15 catalysts are illustrated in Figure 6. Compared with the support (Figure 1(f)), the intensity of the CO_2 desorption peak (Figure 5), corresponding to strong basic sites, was much lower. This could be explained by the high calcination temperature of the catalyst (800°C) while the heating temperature of the SBA-15 support was 550°C and the drying temperature of the NH_3-treated SBA-15 was 120°C. The intense dehydration and Cl^- ion evaporation at the calcination temperature of 800°C resulted in a decrease in the number of Lewis basic sites in the Ni/SBA-15 and NiMg/SBA-15 catalysts. As previously reported, NH_3 was almost completely dissociated from hydrogen and nitrogen at 700°C [35] or 1100°C [40]. Furthermore, the dissociation of NH_3 to N_2 and H_2 was strongly promoted by the Ni catalyst. For example, on the Ni/TiO_2 catalyst, 30% NH_3 was dissociated at 550°C, and almost 100% NH_3 was decomposed at 650°C [34]. These processes led to lowering the basicity of the NH_3-treated catalyst as compared to the corresponding support.

There were two CO_2 desorption peaks in the temperature range of 100–350°C and 400–700°C in all Ni/SBA-15 catalysts. The first peak could be assigned to weak and moderate basic sites while the second one was addressed to strong basic sites. It could be seen that, unlike the support, the majority of basic sites in these catalysts were weak and moderate. Treating NiO/SBA-15 catalysts with $NH_{3(aq)}$ as well as promoting with MgO favoured the presence of weak and moderate basic sites. It followed from Table 1 that the alkalization led to an increase in basic site density. The basicity of the $NH_{3(aq)}$-treated samples on the one hand does not change much when the concentration of $NH_{3(aq)}$ solution changes on the other hand; it is lower than that of the NiMg/SBA-15 catalyst. This may be related to the fact that most of ammonia was dissociated into hydrogen and nitrogen at calcination temperature, and there remained only a small amount of NH_3 residue in the catalysts, as seen in EDS mapping data.

3.2. Catalytic Performance for Bireforming. Figures 7(a) and 7(b) show the activity of Ni/SBA-15 catalysts treated with different $NH_{3(aq)}$ solutions in CH_4 bireforming. It could be seen that both CH_4 and CO_2 conversion increased when raising

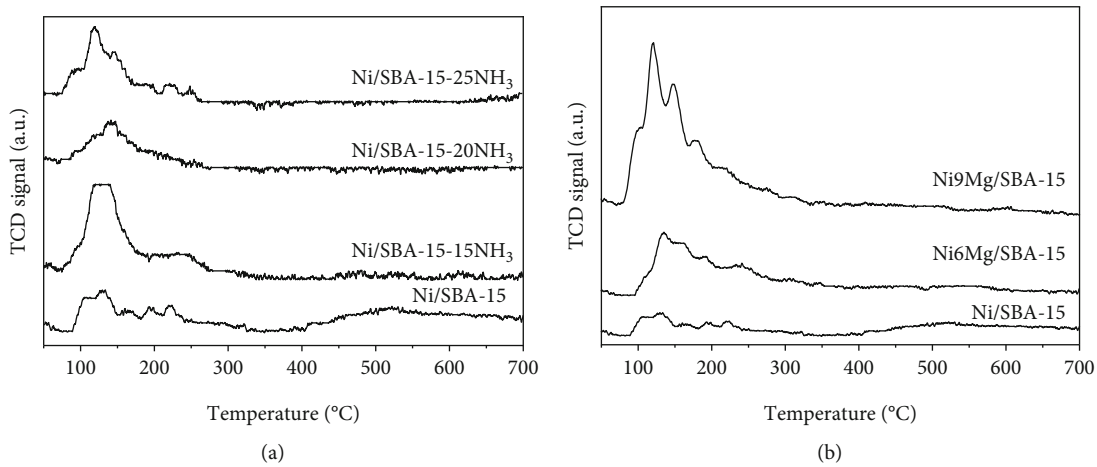

Figure 6: CO_2-TPD pattern of NiO/SBA-15 catalysts alkalized with $NH_{3(aq)}$ (a) and NiO/SBA-15 catalysts promoted by MgO (b).

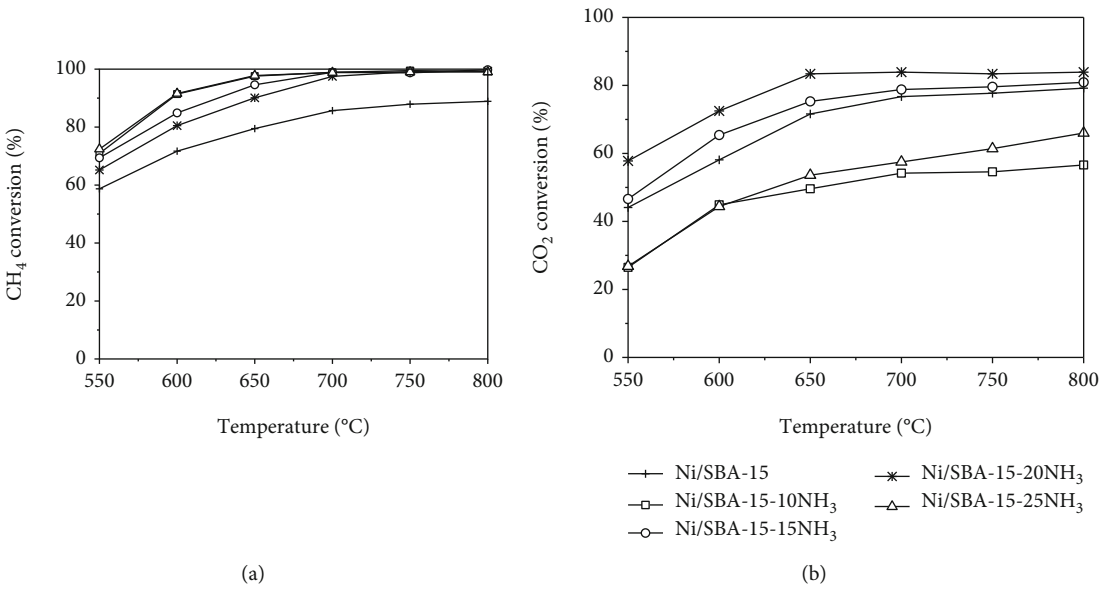

Figure 7: The conversion of CH_4 (a) and CO_2 (b) of NiO/SBA-15 catalysts treated with $NH_{3(aq)}$ at different reaction temperatures.

the reaction temperature. This was evident because bireforming (1) is a strongly endothermic reaction. In general, catalysts showed higher CH_4 conversion than CO_2 conversion. It may be related to the occurrence of the Water Gas Shift (WGS) reaction (4) in methane reforming conditions, producing additional CO_2 [41].

As it was followed from Figures 7 and 8, conversion of CH_4 on modified Ni/SBA-15 catalysts was higher than that on the nonpromoted one over the range of reaction temperature. This might be related to the alkalization of SBA-15 resulting in an increase in NiO dispersion, reducibility, and density of basic sites, as seen in Table 1. Besides, it has been found that the CH_4 conversion of NH_3-modified catalysts was higher than that of the MgO-modified samples. This result could be explained by the higher number of reduced Ni^0 (m_{Ni^0}) in the NH_3-modified catalysts when two groups of modified catalysts were compared. From the data in Figure 8, it could be seen that by increasing the content of MgO additive from 0 to 9%, the CH_4 conversion increased, reaching the maximum value of 96.4% at the content of 9% Mg. However, when Mg content was continually raised to 12%, the conversion of CH_4 slightly decreased.

The magnitude order of the amount of reduced Ni^0, based on H_2-TPR (Table 1), was in the following order:

$$\begin{aligned} &\text{Ni/SBA-15-25NH}_3 > \text{Ni/SBA-15-20NH}_3 \\ &\quad \approx \text{Ni/SBA-15-15NH}_3 > \text{Ni9Mg/SBA-15} \\ &\quad > \text{Ni/SBA-15} > \text{Ni3Mg/SBA-15} > \text{Ni6Mg/SBA-15} \end{aligned} \tag{6}$$

From order (6), it could be seen that four catalysts with the highest number of reduced Ni^0 (Ni/SBA-15-25 NH_3, Ni/SBA-15-20 NH_3, Ni/SBA-15-15 NH_3, and Ni9Mg/SBA-15) were also the samples with the highest CH_4 conversion

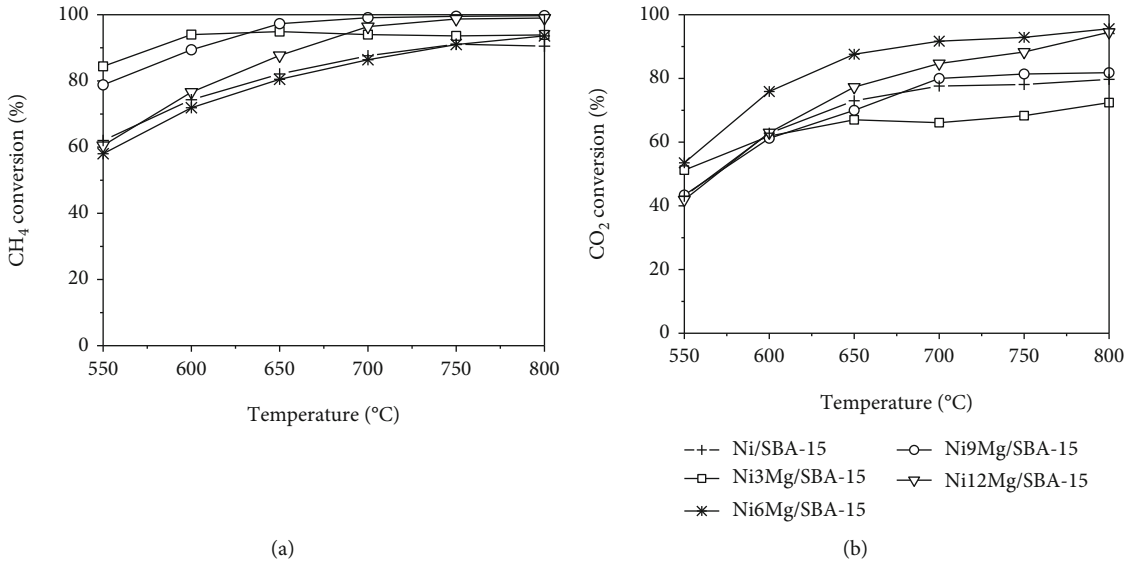

Figure 8: The conversion of CH_4 (a) and CO_2 (b) of NiO/SBA-15 catalysts promoted by MgO at different reaction temperatures.

(Figure 9). The catalysts treated with 15-25% NH_3 had approximately the same and highest value of CH_4 conversion among the catalysts, reaching 98-99% at 700°C because the number of reduced Ni^o of these three catalysts is approximate and the highest. Similarly, in the MgO-promoted catalyst group, the highest CH_4 conversion of the Ni9Mg/SBA-15 sample was due to its highest reducibility. This implied that CH_4 was activated by reduced Ni^o sites, having the higher reducibility catalyst; the higher activity in CH_4 oxidation is reached.

From the obtained results in Table 1, it is possible to order the catalysts based on their basicity as follows:

$$\begin{aligned}&\text{Ni9Mg/SBA-15} > \text{Ni6Mg/SBA-15} > \text{Ni/SBA-15-25 NH}_3\\&> \text{Ni/SBA-15-15 NH}_3 \approx \text{Ni/SBA-15-20 NH}_3\\&\approx \text{Ni3Mg/SBA-15} \approx \text{Ni/SBA-15}\end{aligned} \quad (7)$$

Among the samples, 9% Mg-promoted catalyst showed the highest density of basic sites, and ranked second is the catalyst with 6% Mg, based on the peak area of the TPD pattern. These samples are also the two catalysts with the highest activity in CO_2 conversion. The enhanced basicity was advantageous as CO_2 adsorption affinity could be improved, which in turn affected the CO_2 conversion and stability [42]. However, the dependence of CO_2 conversion on alkalized catalysts with different $NH_{3(aq)}$ solutions was complex (Figure 7(b)). Specifically, CO_2 conversion on the two catalysts alkalized with 15% and 20% $NH_{3(aq)}$ solution was higher than that on the nonalkalized one. In contrast, the catalysts were alkalized with the most dilute (10%) or most concentrated (25%) $NH_{3(aq)}$ solution, exhibiting a lower CO_2 conversion compared to the nonalkalized one. In addition, it should be noted that the catalysts alkalized with 10% and 25% $NH_{3(aq)}$ solution possessed the highest CH_4 conversion and the lowest CO_2 conversion (Figure 7). However, at 700°C and higher, CH_4 conversion was almost the same on the three NH_3-promoted catalysts, reaching over 98%.

It could be observed from Figure 9 that, in most cases, the H_2/CO molar ratio of the product mixture was higher than the theoretical value (which was 2) because of the WGS reaction (4), consuming CO and generating an additional amount of H_2. It was worth noting that when the $NH_{3(aq)}$ concentration or the MgO loading content increased, the H_2/CO ratio decreased and might become less than 2. In addition to the main reaction (1), several side reactions might be involved in the process. The contribution of side reactions in the composition of reaction products was dependent on feed composition and conversion [43] as well as the using catalyst. Some side reactions such as Reverse Water Gas Shift (RWGS) and methane dry reforming (2) reduced the H_2/CO ratio. Alkalization of Ni/SBA-15 catalyst could be able to increase the CO_2 adsorption that would lead to an enhancement of these reactions.

In particular, the Ni/SBA-15-25NH_3 sample has a very low CO_2 conversion although it also has high basicity. The highest CH_4 conversion and the lowest CO_2 conversion obtained on this sample might be related to its highest reducibility, promoting the CH_4 reforming by steam according to Equation (6), with the result of CO_2 additional generation:

$$CH_4 + 2H_2O \rightleftharpoons CO_2 + 4H_2, \quad \Delta H_{298} = +690\,\text{kJ/mol} \quad (8)$$

Further, although possessing higher basicity than Ni6Mg/SBA-15, the Ni9Mg/SBA-15 sample exhibits a slightly lower CO_2 conversion. Additionally, two samples with the highest basicity of the two alkalized catalyst groups (Ni/SBA-15-25NH_3 and Ni9Mg/SBA-15) also expressed the lowest value of mol ratio H_2/CO among the studied catalysts. This is explained as follows. When the samples are treated with a too high loading alkalizing agent, they possess high base properties that enhanced CO_2 adsorption, promoting dry reforming (2), generating more CO. CO in turn activates

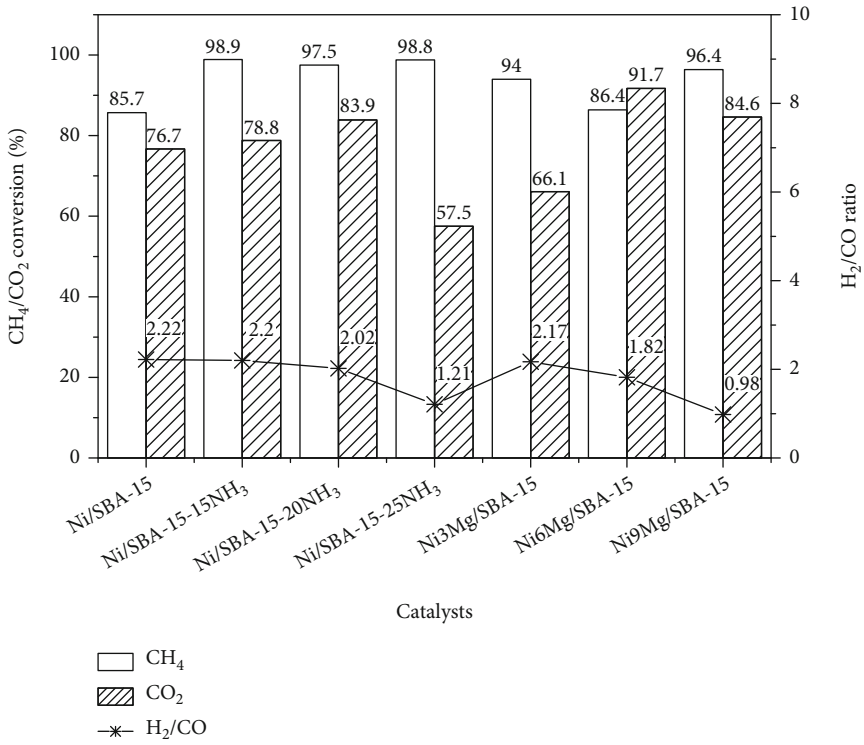

Figure 9: The conversion of CH_4 and CO_2 and the mole ratio H_2/CO at reaction temperatures of 700°C over the catalysts.

the WGS reaction (4), which in result reduces the H_2/CO ratio on the one hand and on the other hand reduces CO_2 conversion. The value of the H_2/CO ratio and the CO_2 conversion depends on the catalyst properties. On the Ni/SBA-15-25NH_3 sample, the WGS reaction (4) was stronger, so the CO_2 conversion was lower, and the H_2 : CO ratio > 1. Conversely, on the Ni9Mg/SBA-15 catalyst, the dry reforming (2) is relatively stronger than WGS reaction (4), so the CO_2 conversion remains quite high, while the ratio H_2/CO~1. In general, excessive alkalization can also lead to disadvantages for the catalysts. Besides, the previous report [44] indicated that excessive basicity of the catalyst itself is detrimental to catalytic activity as it will stimulate a higher extent of the CO_2 dissociation ($CO_2 \rightarrow C + O_2$) and thereupon deactivate the catalyst.

Hence, in order to obtain the highest yield of synthetic gas, it was necessary to select a catalyst with optimal adsorption capacity for these two reactants. Comparison of the two highly active catalysts, Ni/SBA-15-20NH_3 and Ni9Mg/SBA-15, showed that they had an equally high activity with a CH_4 conversion of nearly 97% and a CO_2 conversion of almost 84% at 700°C. However, the H_2/CO ratio obtained remained at 2.02 on the Ni/SBA-15-20NH_3 catalyst and almost 1 on the Ni9Mg/SBA-15 sample. These facts proved that the alkalization of the Ni/SBA-15 catalyst by $NH_{3(aq)}$ solution had an advantage over using MgO because side reactions were unlikely to occur.

As shown in Table 2, there are three main groups of Ni-based catalysts for the BRM reaction based on three supports including Al_2O_3 [14, 49–52, 56], CeO_2 [45, 50, 51], and SBA-15 [9, 42, 52]. In general, the highest value of CH_4 conversion reached on all three groups is

Table 2: Comparison of the CH_4 and CO_2 conversion in CSCRM: reaction temperature (T), CH_4 conversion (X_{CH_4}), and CO_2 conversion (X_{CO_2}).

Catalysts	T (°C)	X_{CH_4} (%)	X_{CO_2} (%)	Refs.
5Ni/Al_2O_3	900	58	—	[45]
5Ni/CeO_2		73	—	
6.67Ni/α-Al_2O_3	700	92	64	[46]
6.67Ni/(MgO-Al_2O_3) (1 : 2)	800	100	67	[47]
6.67Ni/(BaO-Al_2O_3) (1 : 2)		100	78	
6.67Ni/(CaO-Al_2O_3) (1 : 2)		100	58	
Ni/MgO–Al_2O_3	800	93	—	[13]
	700	83	71	
15Ni/$MgAl_2O_4$	850	74	35	[48]
15Ni/CeO_2–ZrO_2/$MgAl_2O_4$		80	41	
15Ni–CeO_2–ZrO_2/$MgAl_2O_4$		81	44	
Ni–Ce/θ-Al_2O_3		80	47	
Ni/$MgAl_2O_4$ (MgO/Al_2O_3 = 3/7)	850	85	47	[49]
Ni–Ce/$MgAl_2O_4$(3)		86	58	
7.87Ni/CeO_2-NR	700	89	67	[50]
	800	96	72	
7.87Ni0.3V/CeO_2-NR	700	96	75	[51]
31.4Ni/SBA-15	700	86	77	[9]
	800	90.5	80	
10Ni/SBA-15	850	98	85	[42]
10Ni3MgO/SBA-15		92	85	
10Ni/Ce-SBA-15	800	78	60	[52]
31.4Ni/SBA-15-20NH_3	700	97	84	This work
31.4Ni9Mg/SBA-15		96	85	

approximately the same, ranging from 86 to 92% at 700°C. Meanwhile, the CO_2 conversion under the same reaction conditions is lower (64-77%). In particular, two groups of Ni catalysts supported on Al_2O_3 and CeO_2 show low CO_2 conversion and do not exceed 67% at 700°C [46, 50], while this value reached 77% on the Ni/SBA-15 catalyst [9]. Furthermore, the promotion of the Ni/Al_2O_3 catalyst by alkali metal additives [13, 47–49] or CeO_2 [48, 49] or Zr [48] did not significantly improve the activity, and the CO_2 conversion did not exceed 78% at 700°C [47]. Meanwhile, for the Ni/CeO_2 catalyst, vanadium additive shows its promoting role, since the conversion of CH_4 and CO_2 at 700°C was raised from 89% to 96% and from 67% to 75%, respectively [51], as 0.3%V was added to the Ni/CeO_2 catalyst. The special feature of the Ni/SBA-15 [9] compared with Ni/Al_2O_3 [46] and Ni/CeO_2 [50] catalysts is that it has high conversion of both CH_4 and CO_2. These values reach 86% and 77% at 700°C, respectively [9]. In comparison with other Ni-based catalysts, Ni/SBA-15-20NH_3 and Ni9Mg/SBA-15 catalysts in this study showed outstanding activity in bireforming of CH_4. Typically, CH_4 conversion on these two samples was almost 97% at 700°C, and CO_2 conversion was nearly 84%, much higher than this value on others.

4. Conclusion

On the one hand, the alkalization of Ni/SBA-15 by NH_3 solution and with MgO promoter led to a sharp decrease in pore diameter, pore volume, and specific surface area, but on the other hand, this modification significantly enhanced the dispersion of NiO particles, reducibility, and basicity of catalysts. As a result, performance of alkalized Ni/SBA-15 catalysts in methane reforming was improved. MgO acted as a highly effective additive for improving the Ni dispersion and enhancing the metal-support parent and the basicity, but it had slight effect on reducibility. Therefore, the Ni/SBA-15 catalyst promoted by MgO exhibited high activity in CO_2 conversion. Meanwhile, the NH_3 treatment led to a homogeneous dispersion of the elements throughout the catalyst. So, the catalyst reducibility as well as CH_4 conversion was improved strongly. However, the excessive alkalization of the catalyst was not favourable in BRM due to strong adsorption of CO_2 and stimulation of side reactions that reduced the H_2/CO ratio. The results revealed that the Ni/SBA-15 treated with 15-25% $NH_{3(aq)}$ solution and promoted with 3-9% Mg exhibited high activity for CH_4 conversion while Ni6Mg/SBA-15 showed the highest CO_2 conversion. Among tested catalysts, Ni/SBA-15-20NH_3 and Ni9Mg/SBA-15 samples showed better catalytic activity. At 700°C, conversion of CH_4 and CO_2 reached 97% and 84%, respectively, on these catalysts, which were higher than the values on the others. However, the Ni/SBA-15-20NH_3 sample showed an advantage in limiting side reactions since the H_2/CO ratio was obtained at a theoretical value.

Data Availability

The data used to support the findings of this study are included within the article.

Conflicts of Interest

The authors declare that there are no conflicts of interest regarding the publication of this paper.

Acknowledgments

This research is funded by Viet Nam National University Ho Chi Minh City (VNU-HCM) under grant number C-2019-20-21.

References

[1] C. Song, "Global challenges and strategies for control, conversion and utilization of CO_2 for sustainable development involving energy, catalysis, adsorption and chemical processing," *Catalysis Today*, vol. 115, no. 1-4, pp. 2–32, 2006.

[2] V. R. Choudhary and A. M. Rajput, "Simultaneous carbon dioxide and steam reforming of methane to syngas over NiO-CaO catalyst," *Industrial & Engineering Chemistry Research*, vol. 35, no. 11, pp. 3934–3939, 1996.

[3] V. Subramani, P. Sharma, L. Zhang, and K. Liu, "Catalytic steam reforming technology for the production of hydrogen and syngas," in *Hydrogen and Syngas Production and Purification Technologies*, K. Liu, C. Song, and V. Subramani, Eds., pp. 14–126, Wiley, 2009.

[4] D. Wang, L. Jin, B. Wei, J. Lv, Y. Li, and H. Hu, "Oxidative catalytic cracking and reforming of coal pyrolysis volatiles over NiO," *Energy & Fuels*, vol. 34, no. 6, pp. 6928–6937, 2020.

[5] C.-C. Hu and H. Teng, "Structural features of p-type semiconducting NiO as a co-catalyst for photocatalytic water splitting," *Journal of Catalysis*, vol. 272, no. 1, pp. 1–8, 2010.

[6] X. Li, Y. Wang, J. Wang et al., "Sequential electrodeposition of bifunctional catalytically active structures in MoO_3/Ni–NiO composite electrocatalysts for selective hydrogen and oxygen evolution," *Advanced Materials*, vol. 32, no. 39, p. 2003414, 2020.

[7] H.-S. Roh, K.-W. Jun, S.-C. Baek, and S.-E. Park, "A highly active and stable catalyst for carbon dioxide reforming of methane: $Ni/Ce–ZrO_2/\theta$-Al_2O_3," *Catalysis Letters*, vol. 81, no. 3/4, pp. 147–151, 2002.

[8] G. Zhang, L. Hao, Y. Jia, and Y. Zhang, "CO_2 reforming of CH_4 over efficient bimetallic Co-Zr/AC catalyst for H_2 production," *International Journal of Hydrogen Energy*, vol. 40, no. 37, pp. 12868–12879, 2015.

[9] P. H. Phuong, L. C. Loc, H. T. Cuong, and N. Tri, "Effect of NiO loading and thermal treatment duration on performance of Ni/SBA-15 catalyst in combined steam and CO_2 reforming of CH_4," *Materials Transactions*, vol. 59, no. 12, pp. 1898–1902, 2018.

[10] M. Zhang, S. Ji, L. Hu, F. Yin, C. Li, and H. Liu, "Structural characterization of highly stable Ni/SBA-15 catalyst and its catalytic performance for methane reforming with CO_2," *Chinese Journal of Catalysis*, vol. 27, no. 9, pp. 777–781, 2006.

[11] M. A. Soria, C. Mateos-Pedrero, A. Guerrero-Ruiz, and I. Rodríguez-Ramos, "Thermodynamic and experimental study of combined dry and steam reforming of methane on Ru/ ZrO_2-La_2O_3 catalyst at low temperature," *International Journal of Hydrogen Energy*, vol. 36, no. 23, pp. 15212–15220, 2011.

[12] H.-S. Roh and K.-W. Jun, "Carbon dioxide reforming of methane over Ni catalysts supported on Al_2O_3 modified with La_2O_3, MgO, and CaO," *Catalysis Surveys from Asia*, vol. 12, no. 4, pp. 239–252, 2008.

[13] H.-S. Roh, K. Y. Koo, J. H. Jeong et al., "Combined reforming of methane over supported Ni catalysts," *Catalysis Letters*, vol. 117, no. 1-2, pp. 85–90, 2007.

[14] J. Juan-Juan, M. C. Román-Martínez, and M. J. Illán-Gómez, "Effect of potassium content in the activity of K-promoted Ni/Al_2O_3 catalysts for the dry reforming of methane," *Applied Catalysis A: General*, vol. 301, no. 1, pp. 9–15, 2006.

[15] M. M. Danilova, Z. A. Fedorova, V. A. Kuzmin, V. I. Zaikovskii, A. V. Porsin, and T. A. Krieger, "Combined steam and carbon dioxide reforming of methane over porous nickel based catalysts," *Catalysis Science & Technology*, vol. 5, no. 5, pp. 2761–2768, 2015.

[16] N. Wang, X. Yu, K. Shen, W. Chu, and W. Qian, "Synthesis, characterization and catalytic performance of MgO-coated Ni/SBA-15 catalysts for methane dry reforming to syngas and hydrogen," *International Journal of Hydrogen Energy*, vol. 38, no. 23, pp. 9718–9731, 2013.

[17] Z. Alipour, M. Rezaei, and F. Meshkani, "Effect of alkaline earth promoters (MgO, CaO, and BaO) on the activity and coke formation of Ni catalysts supported on nanocrystalline Al_2O_3 in dry reforming of methane," *Journal of Industrial and Engineering Chemistry*, vol. 20, no. 5, pp. 2858–2863, 2014.

[18] E. Ruckenstein and Y. H. Hu, "Methane partial oxidation over NiO/MgO solid solution catalysts," *Applied Catalysis A: General*, vol. 183, no. 1, pp. 85–92, 1999.

[19] Y.-H. Wang, H.-M. Liu, and B.-Q. Xu, "Durable Ni/MgO catalysts for CO_2 reforming of methane: activity and metal-support interaction," *Journal of Molecular Catalysis A: Chemical*, vol. 299, no. 1-2, pp. 44–52, 2009.

[20] S. J. H. Rad, M. Haghighi, A. A. Eslami, F. Rahmani, and N. Rahemi, "Sol-gel vs. impregnation preparation of MgO and CeO_2 doped Ni/Al_2O_3 nanocatalysts used in dry reforming of methane: Effect of process conditions, synthesis method and support composition," *International Journal of Hydrogen Energy*, vol. 41, no. 11, pp. 5335–5350, 2016.

[21] K. Selvarajah, N. H. H. Phuc, B. Abdullah, F. Alenazey, and D.-V. N. Vo, "Syngas production from methane dry reforming over Ni/Al_2O_3 catalyst," *Research on Chemical Intermediates*, vol. 42, no. 1, pp. 269–288, 2016.

[22] L. You, F. Yuan, and F. Ma, "Synthesis of mesoporous NH2-SBA-15 by a simple and efficient strategy," *Russian Journal of Physical Chemistry A*, vol. 89, no. 12, pp. 2298–2303, 2015.

[23] Z. Hao, Q. Zhu, Z. Jiang, and H. Li, "Fluidization characteristics of aerogel Co/Al_2O_3 catalyst in a magnetic fluidized bed and its application to CH_4-CO_2 reforming," *Powder Technology*, vol. 183, no. 1, pp. 46–52, 2008.

[24] S. N. Bukhari, C. Y. Chin, H. D. Setiabudi, and D.-V. N. Vo, "Tailoring the properties and catalytic activities of Ni/SBA-15 via different TEOS/P123 mass ratios for CO_2 reforming of CH_4," *Journal of Environmental Chemical Engineering*, vol. 5, no. 4, pp. 3122–3128, 2017.

[25] M. S. M. d. Oliveira, L. Bieseki, A. E. V. d. Alencar, T. P. Braga, and S. B. C. Pergher, "Incorporating aluminum into the structure of SBA-15 by adjusting the pH and adding NaF," *Materials Research*, vol. 22, no. 3, 2019.

[26] B. M. Q. Phan, Q. L. M. Ha, N. P. Le et al., "Influences of various supports, γ-Al_2O_3, CeO_2, and SBA-15 on HDO performance of NiMo catalyst," *Catalysis Letters*, vol. 145, no. 2, pp. 662–667, 2015.

[27] H. Zhang, M. Li, P. Xiao, D. Liu, and C. J. Zou, "Structure and catalytic performance of Mg-SBA-15-supported nickel catalysts for CO_2 Reforming of methane to syngas," *Chemical Engineering & Technology*, vol. 36, no. 10, pp. 1701–1707, 2013.

[28] E. P. Perman, G. A. S. Atkinson, and W. Ramsay, "The decomposition of ammonia by heat," *Proceedings of the Royal Society of London*, vol. 74, no. 497-506, pp. 110–117, 1905.

[29] H. Li, J. Ren, X. Qin, Z. Qin, J. Lin, and Z. Li, "Ni/SBA-15 catalysts for CO methanation: effects of V, Ce, and Zr promoters," *RSC Advances*, vol. 5, no. 117, pp. 96504–96517, 2015.

[30] H. Setiabudi, N. Razak, F. Suhaimi, and F. Pauzi, "CO_2 reforming of CH_4 over Ni/SBA-15: influence of Ni-loading methods," *Malaysian Journal of Catalysis*, vol. 1, 2016.

[31] C. C. Chong, L. P. Teh, and H. D. Setiabudi, "Syngas production via CO2 reforming of CH4 over Ni-based SBA-15: promotional effect of promoters (Ce, Mg, and Zr)," *Materials Today Energy*, vol. 12, pp. 408–417, 2019.

[32] A. L. Patterson, "The Scherrer formula for X-ray particle size determination," *Physical review*, vol. 56, no. 10, pp. 978–982, 1939.

[33] A. J. Vizcaíno, A. Carrero, and J. A. Calles, "Ethanol steam reforming on Mg- and Ca-modified Cu-Ni/SBA-15 catalysts," *Catalysis Today*, vol. 146, no. 1-2, pp. 63–70, 2009.

[34] K. Okura, K. Miyazaki, H. Muroyama, T. Matsui, and K. Eguchi, "Ammonia decomposition over Ni catalysts supported on perovskite-type oxides for the on-site generation of hydrogen," *RSC Advances*, vol. 8, no. 56, pp. 32102–32110, 2018.

[35] T. Saika, M. Nakamura, T. Nohara, and S. Ishimatsu, "Study of hydrogen supply system with ammonia fuel," *JSME International Journal Series B Fluids and Thermal Engineering*, vol. 49, no. 1, pp. 78–83, 2006.

[36] D. Xu, W. Li, Q. Ge, and H. Xu, "A novel process for converting coalmine-drained methane gas to syngas over nickel-magnesia solid solution catalysts," *Fuel Processing Technology*, vol. 86, no. 9, pp. 995–1006, 2005.

[37] T. Yoshida, T. Tanaka, H. Yoshida, T. Funabiki, and S. Yoshida, "Study on the dispersion of nickel ions in the NiO– MgO system by X-ray absorption fine structure," *The Journal of Physical Chemistry*, vol. 100, no. 6, pp. 2302–2309, 1996.

[38] D. Li, L. Zeng, X. Li et al., "Ceria-promoted Ni/SBA-15 catalysts for ethanol steam reforming with enhanced activity and resistance to deactivation," *Applied Catalysis B: Environmental*, vol. 176-177, pp. 532–541, 2015.

[39] Z. Bian, Z. Li, J. Ashok, and S. Kawi, "A highly active and stable Ni–Mg phyllosilicate nanotubular catalyst for ultrahigh temperature water-gas shift reaction," *Chemical Communications*, vol. 51, no. 91, pp. 16324–16326, 2015.

[40] A. H. White and W. Melville, "The decomposition of ammonia at high temperatures," *Journal of the American Chemical Society*, vol. 27, no. 4, pp. 373–386, 1905.

[41] S. Wang, G. Q. M. Lu, and G. J. Millar, "Carbon dioxide reforming of methane to produce synthesis gas over metal-supported catalysts: state of the art," *Energy & Fuels*, vol. 10, no. 4, pp. 896–904, 1996.

[42] B. Huang, X. Li, S. Ji, B. Lang, F. Habimana, and C. Li, "Effect of MgO promoter on Ni-based SBA-15 catalysts for combined

steam and carbon dioxide reforming of methane," *Journal of Natural Gas Chemistry*, vol. 17, no. 3, pp. 225–231, 2008.

[43] M. M. B. Quiroga and A. E. C. Luna, "Kinetic analysis of rate data for dry reforming of methane," *Industrial & Engineering Chemistry Research*, vol. 46, no. 16, pp. 5265–5270, 2007.

[44] S. Das, M. Sengupta, J. Patel, and A. Bordoloi, "A study of the synergy between support surface properties and catalyst deactivation for CO_2 reforming over supported Ni nanoparticles," *Applied Catalysis A: General*, vol. 545, pp. 113–126, 2017.

[45] N. Laosiripojana, D. Chadwick, and S. Assabumrungrat, "Effect of high surface area CeO2 and Ce- ZrO2 supports over Ni catalyst on CH4 reforming with H2O in the presence of O2, H2, and CO2," *Chemical Engineering Journal*, vol. 138, no. 1-3, pp. 264–273, 2008.

[46] P. H. Phuong, L. C. Loc, D. N. Tin et al., "Combined steam and CO_2 reforming of CH_4 over NiO/αAl2O_3 catalysts promoted with MgO and V_2O_5," *Vietnam Journal of Chemistry*, vol. 55, no. 5e34, pp. 181–185, 2017.

[47] P. H. Phuong, L. C. Loc, P. T. Sang, and N. Tri, "Combined steam and CO_2 reforming of CH_4 over nickel catalysts based on Al_2O_3–MO (M= Mg, Ca, Ba)," *Vietnam Journal of Science and Technology*, vol. 55, 2018.

[48] J. W. Bae, A. R. Kim, S.-C. Baek, and K.-W. Jun, "The role of CeO_2–ZrO_2 distribution on the Ni/$MgAl_2O_4$ catalyst during the combined steam and CO_2 reforming of methane," *Reaction Kinetics, Mechanisms and Catalysis*, vol. 104, no. 2, pp. 377–388, 2011.

[49] S.-C. Baek, J.-W. Bae, J. Y. Cheon, K.-W. Jun, and K.-Y. Lee, "Combined steam and carbon dioxide reforming of methane on Ni/$MgAl_2O_4$: effect of CeO_2 promoter to catalytic performance," *Catalysis Letters*, vol. 141, no. 2, pp. 224–234, 2011.

[50] L. C. Loc, P. H. Phuong, D. Putthea, N. Tri, N. T. T. Van, and H. T. Cuong, "Effect of CeO_2 morphology on performance of NiO/CeO_2 catalyst in combined steam and CO_2 reforming of CH_4," *International Journal of Nanotechnology*, vol. 15, no. 11/12, pp. 968–982, 2018.

[51] P. H. Phuong, L. C. Loc, N. Tri et al., "Effect of V_2O_5 promoter on characteristics and performance of NiO/CeO_2 catalyst in methane bi-reforming," *Advances in Natural Sciences: Nanoscience and Nanotechnology*, vol. 11, no. 4, 2020.

[52] J. S. Tan, H. T. Danh, S. Singh, Q. D. Truong, H. D. Setiabudi, and D.-V. N. Vo, "Syngas production from CO2reforming and CO_2-steam reforming of methane over Ni/Ce-SBA-15 catalyst," *IOP Conference Series: Materials Science and Engineering*, vol. 206, 2017.